RADIATIVE SHOCK SOLUTIONS WITH MULTIGROUP DISCRETE-ORDINATES TRANSPORT

An Undergraduate Research Scholars Thesis

by

AARON MIGUEL HOLGADO

Submitted to Honors and Undergraduate Research
Texas A&M University
in partial fulfillment of the requirements for the designation as

UNDERGRADUATE RESEARCH SCHOLAR

Approved by
Research Advisor: Ryan G. McClarren

May 2014

Major: Nuclear Engineering

TABLE OF CONTENTS

Page

ABSTRACT

Radiative Shock Solutions with Multigroup Discrete-Ordinates Transport. (May 2014)

Aaron Miguel Holgado
Department of Nuclear Engineering
Texas A&M University

Research Advisor: Dr. Ryan G. McClarren
Department of Nuclear Engineering

We obtain semi-analytic planar radiative shock solutions using a multigroup discrete-ordinates (S_n) radiation transport model. Comparisons are made to the grey nonequilibrium diffusion solutions of Lowrie and Edwards and the grey-S_n transport solutions of Ferguson, Morel, and Lowrie. Our solutions can be used to verify radiation-hydrodynamics codes. The material opacity is assumed to be constant and we apply a multigroup discretization to the $\mathcal{O}(u/c)$ steady-state frequency-integrated S_n transport equation in order to investigate the structure of the group radiation temperatures. From the structures of the group radiation temperatures, we show that anti-diffusive-like behavior can be due to frequency dependence of the Planck function and not just the angular dependence of the radiation field.

DEDICATION

This work is dedicated to my father and mother. They have pushed me to always strive for excellence and their constant support has kept me motivated.

ACKNOWLEDGMENTS

I would like to thank Dr. McClarren for taking me in as his student for research and for motivating my interest in high-energy-density physics. I would also like to thank Jim Ferguson for his exceptional guidance in not just academics but life in general.

NOMENCLATURE

EOS	Equation of State
S_n	Discrete-Ordinates
HED	High-Energy-Density
ODE	Ordinary Differential Equation
RHD	Radiation Hydrodynamics
VEF	Variable Eddington Factor

CHAPTER I

INTRODUCTION

Several decades ago, developments to the understanding of astrophysics could only be made through theory and observation. High-energy-density (HED) conditions are now attainable in the laboratory and data from these experiments has provided insight into astrophysics and inertial confinement fusion. In astrophysical settings or HED conditions, there may be electromagnetic radiation present in the medium that affects its dynamics. This regime of fluid flow is known as radiation-hydrodynamics (RHD). A radiative shock is a shock wave in which the electromagnetic radiation affects the hydrodynamic evolution of the shock's structure and propagation through a medium [1]. Radiative shock calculations are a vital supplement for the design and analysis of HED experiments. Model improvements of radiative shocks allows for a better understanding behind the physics of supernova and inertial confinement fusion. The extensive use of RHD codes for simulation of HED phenomena has required verification in order to ensure accuracy of the simulations. One method of code verification is deriving semi-analytic solutions to the mathematical model. The solutions are referred to as semi-analytic because they are derived analytically, but must be solved numerically. Previous semi-analytic solutions were obtained by Lowrie and Rauenzahn where they showed the continuity of radiative shocks in the equilibrium diffusion limit [4]. This model was then extended to grey non-equilibrium diffusion by Lowrie and Edwards, where they explicitly showed the existence of the Zel'dovich spike [3]. The radiative shock model was then extended by Ferguson, Morel, and Lowrie (in preparation) to describe the radiation field using S_n transport instead of diffusion [2]. This led to the confirmation of anti-diffusive behavior of the radiation temperature in the cooling layer of the radiative shock, which was predicted by McClarren and Drake [5]. This work implements multigroup-S_n transport for obtaining radiative shock solutions, which extends the work done by Ferguson where additional relevant references and details can be found [2]. As shown by previous literature, not much has been done to study material frequency dependence and its effects on radiative

shock structure [4, 3, 2, 8]. Numerical simulations, however, have been done by Vaytet et al. where they use a multigroup-RHD numerical model to calculate radiative shocks, where they show anti-diffusive-like behavior and an extended precursor region due to frequency dependence [8]. This work further investigates anti-diffusive-like behavior and confirms whether or not it can be a result of frequency dependence of the Planck function and not just angular dependence of the radiation field. The mathematical model is implemented with the Python programming language and the results are analyzed for a frequency-independent opacity.

Nondimensionalization

Whenever dealing with systems of equations that depend on many variables and parameters, it is convenient to work with nondimensional quantities. A tilde (˜) above the parameter denotes that it is a dimensional quantity. The reference quantities used are

$\tilde{L}$	reference length
$\tilde{a}_0$	reference material sound speed
$\tilde{\rho}_0$	reference material mass density
$\tilde{c}$	speed of light
$\tilde{T}_0$	reference material temperature
$\tilde{a}_r$	radiation constant
$\tilde{h}$	Planck's constant
$\tilde{k}_B$	Boltzmann's constant

which are used to define the following nondimensional quantities

$$x = \frac{\tilde{x}}{\tilde{L}} \quad \text{(spatial coordinate)}$$
$$t = \frac{\tilde{t}\tilde{a}_0}{\tilde{L}} \quad \text{(temporal coordinate)}$$
$$\rho = \frac{\tilde{\rho}}{\rho_0} \quad \text{(material mass density)}$$

$$u = \frac{\tilde{u}}{\tilde{a_0}} \text{ (velocity)}$$
$$\mathbb{C} \equiv \frac{\tilde{c}}{\tilde{a_0}}$$
$$\beta = \frac{\tilde{u}}{\tilde{c}} = u\frac{\tilde{a_0}}{\tilde{c}} = \frac{u}{\mathbb{C}}$$
$$e = \frac{\tilde{e}}{\tilde{a_0^2}} \text{ (material internal specific energy)}$$
$$P = \frac{\tilde{P}}{\tilde{\rho_0}\tilde{a_0^2}} \text{ (material pressure)}$$
$$T = \frac{\tilde{T}}{\tilde{T_0}} \text{ (material temperature)}$$
$$\theta = \frac{\tilde{\theta}}{T_0} \text{ (radiation temperature)}$$
$$\sigma_a = \tilde{\sigma_a}\tilde{L} \text{ (absorption cross-section)}$$
$$\sigma_s = \tilde{\sigma_s}\tilde{L} \text{ (scattering cross-section)}$$
$$\sigma_t = \tilde{\sigma_s}\tilde{L} \text{ (total cross-section)}$$
$$\mathbb{P} \equiv \frac{\tilde{a_R}\tilde{T_0^4}}{\tilde{\rho_0}\tilde{a_0^2}}$$
$$E_r = \frac{\tilde{E_r}}{\tilde{a_R}\tilde{T_0^4}} \text{ (radiation energy density)}$$
$$F_r = \frac{\tilde{F_r}}{\tilde{a_R}\tilde{c}\tilde{T_0^4}} \text{ (radiation flux)}$$
$$P_r = \frac{\tilde{P_r}}{\tilde{a}_R\tilde{T_0^4}} \equiv fE_r \text{ (radiation pressure)}$$
$$I_\nu = \frac{\tilde{a}_R\tilde{c}\tilde{h}\tilde{T_\infty^3}}{\tilde{k_B}}\tilde{I}_\nu \text{ (frequency-dependent radiation intensity)}$$
$$B_\nu = \frac{\tilde{a}_R\tilde{c}\tilde{h}\tilde{T_\infty^3}}{\tilde{k_B}}\tilde{B}_\nu \text{ (Planck function) .}$$

The variable Eddington factor (VEF), f, relates the radiation energy to the radiation pressure and is used to close the radiation variable relations. The VEF is later defined in the *Radiative Transfer* section.

Governing Equations

Hydrodynamics

We consider a regime of RHD where the fluid is compressible and the viscosity is assumed to be negligible. This is reasonable because the ion mean-free-path, which sets the material shock's length scale, is considerably smaller than the photon mean-free-path, which establishes the spatial structure of the radiative shock. For inviscid fluid flow, the Euler equations are used to describe the hydrodynamics. This study focuses on planar shocks; thus, we consider spatial variation of fluid properties in the x-direction. In the regime of nonrelativistic RHD, the 1-D nondimensional hydrodynamic model that describes the evolution of the material properties is given by

$$\partial_t \rho + \partial_x(\rho u) = 0 \ , \tag{I.1a}$$

$$\partial_t(\rho u) + \partial_x(\rho u^2 + P) = -\mathbb{P} S_{\text{rp}} \ , \tag{I.1b}$$

$$\partial_t\left(\rho e + \frac{1}{2}\rho u^2\right) + \partial_x\left[u\left(\frac{1}{2}\rho u^2 + \rho e + P\right)\right] = -\mathbb{P}\mathbb{C} S_{\text{re}} \ , \tag{I.1c}$$

where ρ is the material density, u is the material velocity, P is the pressure, and e is the material internal specific energy. The source terms S_{rp} and S_{re} represent the contribution of momentum and energy, respectively, of the radiation to the material and are later defined in the following subsection. The equations of the system, (I.1a)-(I.1c), represents the conservation of mass, total momentum, and total energy, respectively, for the material. The constant, $\mathbb{P}$, is a measure of the radiation effects on flow dynamics and is proportional to the ratio of radiation pressure to material pressure. It is also proportional to the ratio of radiation energy to material energy. The constant, $\mathbb{C}$, is the ratio of the speed of light to the speed of sound in the medium and can therefore be considered to be a measure of relativistic effects. The material internal energy equation can be derived by subtracting the material kinetic energy from the material total energy equation (I.1c)

$$\rho \partial_t e + u \partial_x e + P \partial_x u = \mathbb{P}\sigma_a(E_r - T^4) \ , \tag{I.2}$$

where σ_a is the absorption cross section of the material, T is the material temperature, and E_r is the radiation energy density, which is defined in the following section.

Radiative Transfer

The specific intensity, I, depends on space, frequency, direction, and time, which is denoted as $I(\vec{r}, \nu, \Omega, t)$. The specific intensity is the most fundamental quantity that describes the radiation field of a given volume and has units of $[MeV/(cm^2 - s - str - Hz)]$. The specific intensity will be referred to as the radiation intensity for the rest of this work. In the 1-D case, spatial variation occurs along the x-direction and we use the direction cosine, $\mu \equiv cos\theta$, where $0 \leq \theta \leq 180°$, such that $-1 \leq \mu \leq 1$, to describe the net macroscopic flow of the radiation field through the fluid. This modifies the radiation intensity into $I = I(x, \nu, \mu, t) = I_\nu(x, \mu, t)$. The zeroth, first, and second angular-moments of the nondimensional radiation intensity provide additional quantities that can be used to describe the radiation field and are given by

$$\phi_\nu \equiv 2\pi \int_{-1}^{1} I_\nu \, d\mu \ , \tag{I.3a}$$

$$F_\nu \equiv 2\pi \int_{-1}^{1} \mu I_\nu \, d\mu \ , \tag{I.3b}$$

$$P_\nu \equiv 2\pi \int_{-1}^{1} \mu^2 I_\nu \, d\mu \ , \tag{I.3c}$$

where ϕ_ν is the angle-integrated radiation intensity, F_ν is the frequency-dependent radiation flux, and P_ν is the frequency-dependent radiation pressure. Integrating these quantities over all frequencies yields

$$E_r = 2\pi \int_0^\infty \int_{-1}^{1} I_\nu \, d\nu d\mu \ , \tag{I.4a}$$

$$F_r = 2\pi \int_0^\infty \int_{-1}^{1} \mu I_\nu \, d\nu d\mu \ , \tag{I.4b}$$

$$P_r = 2\pi \int_0^\infty \int_{-1}^{1} \mu^2 I_\nu \, d\nu d\mu \ , \tag{I.4c}$$

where E_r is the radiation energy density, F_r is the radiation flux, and P_r is the radiation pressure. The radiative transfer equation is given by

$$\left(\partial_t + \hat{\mathbf{n}} \cdot \nabla\right) I(\nu, \hat{\mathbf{n}}) = S(\nu, \hat{\mathbf{n}}) \ , \tag{I.5}$$

where $I(\nu, \hat{\mathbf{n}})$ is the photon intensity and $S(\nu, \hat{\mathbf{n}})$ is a source term for the photons. The full radiative transfer equation states that for any given phase space element, the changes in radiation intensity are due to sources, scattering, and losses in that element [1, 7]. In this work, only absorption interactions between the material and the radiation are treated. By treating the photons as particles, a 1-D radiation transport equation can be derived in the form of a Boltzmann equation that describes radiation-material interactions accounting for material motion

$$\partial_t I_\nu + \mu \partial_x I_\nu = -\frac{\nu_o}{\nu} \sigma_t I_\nu + \left(\frac{\nu}{\nu_o}\right)^2 \int_{4\pi} \frac{\nu_o}{\nu'} I_{\nu'}(\mu') \ d\mu' + \left(\frac{\nu}{\nu_o}\right)^2 \sigma_a B_\nu(T) \ , \tag{I.6}$$

where the subscript-o indicates a co-moving frame quantity. This form of the radiation transport equation assumes that the material is in local thermodynamic equilibrium. This means that the radiation emitted by the material will take the form of blackbody radiation, which is suggested by the Planck term. The nondimensional Planck term, $B(\nu, T)$, is the isotropic specific intensity in thermal equilibrium and is given by

$$B(\nu, T) = \frac{2k_B^4}{a_R c^3 h^3} \left(e^{(\nu/T)} - 1\right)^{-1} . \tag{I.7}$$

The Planckian distribution characterizes the radiation emitted by a black body at a given temperature [6]. The nondimensional radiation source-rates of energy, momentum, and internal energy are

$$S_{\text{re}} = \sigma_a(T^4 - E_r) + \beta(\sigma_a - \sigma_s)F_r + \beta^2[(\sigma_s - \sigma_a)(E_r + P_r) + \sigma_a(T^4 - E_r)] = \partial_x F_r \ , \tag{I.8a}$$

$$S_{\text{rp}} = -\sigma_t[F_r - \beta(E_r + P_r)] + \sigma_a \beta(T^4 - E_r) = \partial_x P_r \ , \tag{I.8b}$$

$$S_{\rm re} - \beta S_{\rm rp} = \sigma_a(T^4 - E_r) + 2\sigma_a\beta(F_r - E_r - P_r) \ . \tag{I.8c}$$

The source terms, $S_{\rm re}$ and $S_{\rm rp}$, couple the effects of radiation to the flow dynamics. The radiation travels through the material in every direction in differing amounts. The Eddington factor, f, measures the angular variation of the radiation and is a measure of the anisotropy of the specific intensity [9]. In previous work [4, 3], f has been defined as $f(x) \equiv 1/3$, which indicates that the radiation field emits isotropically and thus behaves diffusively. For this work, f is treated as a variable Eddington factor (VEF) in the same manner as was done by Ferguson [2]

$$f \equiv \frac{\int_{4\pi} \mu^2 I(\mu)\ d\mu}{\int_{4\pi} I(\mu)\ d\mu} = \frac{P_r}{E_r} \ . \tag{I.9}$$

Using the material-motion-corrected radiation transport equation (I.6), we obtain a nonrelativistic transport model that describes the evolution of radiation. The steady-state lab-frame frequency-dependent 1-D radiation transport equation, Taylor expanded through $O(\beta)$, is

$$\begin{aligned} \mu\partial_x I_\nu = \frac{\sigma_s}{4\pi}E_\nu + \sigma_a B_\nu - \sigma_t I_\nu - \frac{\sigma_s}{4\pi}\beta(F_\nu - \nu\partial_\nu F_\nu) \\ +\mu\beta\left[\sigma_t I_\nu + I_\nu\nu\partial_\nu\sigma_t + 2\frac{\sigma_s}{4\pi}E_\nu + 2\sigma_a B_\nu - \frac{\sigma_s}{4\pi}\nu\partial_\nu E_\nu - \nu\partial_\nu(\sigma_a B_\nu)\right] \ , \end{aligned} \tag{I.10}$$

and is solved in this work using the multigroup and S_n radiation transport models.

Multigroup Approximation of Frequency Dependence

The opacity of a material describes how likely it is to interact with photons, or a measure of how "opaque" it is to electromagnetic radiation. In general, the opacity of a material is highly dependent on frequency. The main focus of this work is implementing the multigroup method to capture the frequency dependence of the Planck function. Previously, grey transport has been used for obtaining radiative shock profiles [2], which assumes a frequency-independent opacity. An example of a frequency-dependent opacity profile is given in Figure I.1.

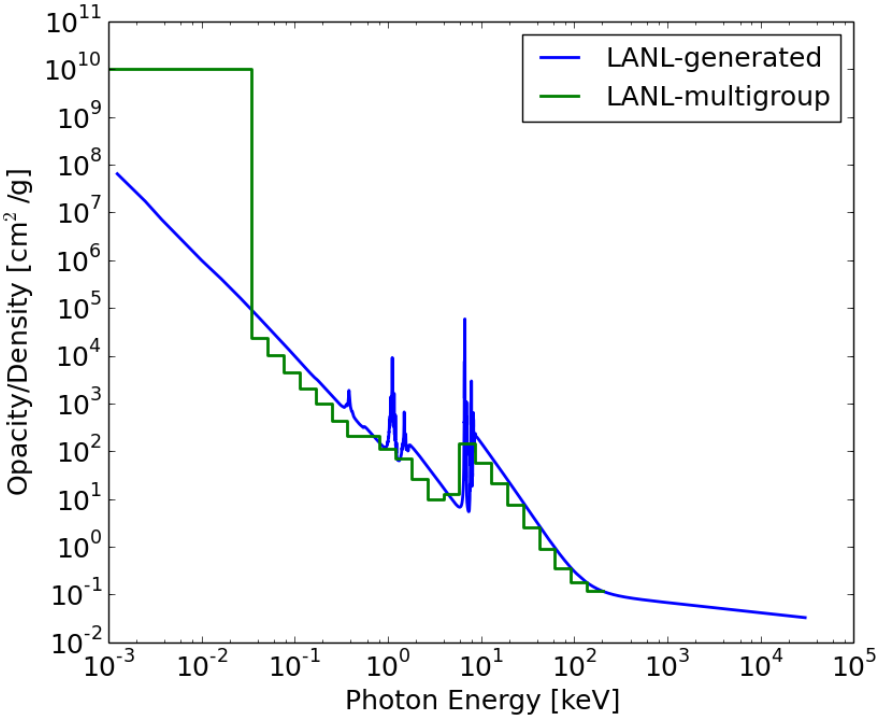

Fig. I.1. Opacity of iron overlayed with multigroup representation using 33 groups. Data obtained from Los Alamos National Laboratory opacity database.

One of the bulk features of the iron opacity is that it is linear when plotted on a log-log scale. Thus, the material's tendency to interact with the radiation decreases exponentially as a photon's energy increases. Other noticable features in Figure I.1 are the lines and edges. These structures are mainly due to electronic transitions that the material can undergo when it interacts with radiation. The placement of the group boundaries is up to the user's preferences in terms of resolving the regions where the opacity peaks and jumps in relatively small ranges. It is expected that using the multigroup method will provide better insight into the role of these features than the grey approximation does. The multigroup method

involves discretizing the frequency domain into a number of groups, G, and integrating a frequency-dependent variable of interest as

$$x_g = \int_{\nu_g}^{\nu_{g+1}} x_\nu \, d\nu \ . \tag{I.11}$$

Using one group for solving multigroup transport is equivalent to solving grey transport. If the group boundaries are equally spaced over the frequency domain for any number of groups, then increasing the number of groups will decrease the width of each group, which captures more information of the opacity.

Frequency Dependence of Radiation Variables

Applying the multigroup approximation to the frequency-dependent radiation variables yields

$$E_g = \int_{\nu_g}^{\nu_{g+1}} \phi_\nu \, d\nu \ , \tag{I.12}$$

$$F_g = \int_{\nu_g}^{\nu_{g+1}} F_\nu d\nu \ , \tag{I.13}$$

$$P_g = \int_{\nu_g}^{\nu_{g+1}} P_\nu d\nu \ , \tag{I.14}$$

where E_g, F_g, and P_g, are the group-averaged radiation energy density, flux, and pressure, respectively. The radiation variables can then be re-expressed as sums of their respective group-averaged quantities:

$$E_r = \sum_{g=1}^{G} E_g \ , \tag{I.15}$$

$$F_r = \sum_{g=1}^{G} F_g \ , \tag{I.16}$$

$$P_r = \sum_{g=1}^{G} P_g \ . \tag{I.17}$$

RHD Model

Coupling the steady-state hydrodynamics and radiation transport models and implementing the multigroup frequency approximation yields the 1-D multigroup RHD equations which consist of the Euler equations and the material internal specific energy equation

$$\partial_x(\rho u) = 0 \ , \tag{I.18a}$$

$$\partial_x(\rho u^2 + P + \mathbb{P}P_r) = 0 \ , \tag{I.18b}$$

$$\partial_x\left[u\left(\frac{1}{2}\rho u^2 + \rho e + P\right) + \mathbb{P}\mathbb{C}F_r\right] = 0 \ , \tag{I.18c}$$

$$\rho u\partial_x e + P\partial_x u = -\mathbb{P}\mathbb{C}[\sigma_a(T^4 - E_r) + 2\sigma_a\beta(F_r - E_r - P_r)] \ , \tag{I.18d}$$

and the multigroup radiation transport equation

$$\begin{aligned}\mu\partial_x I_g = {} & \frac{\sigma_s}{4\pi}\phi_g + \sigma_{a,P}B_g - \sigma_{t,P}I_g - 2\frac{\sigma_s}{4\pi}\beta F_g + \frac{\sigma_s}{4\pi}\beta\left(\nu F_\nu|_{\partial g}\right) \\ & + \mu\beta\left[\sigma_{t,P}I_g + I_g(\nu\partial_\nu\sigma_t)_{g,P} + 3\frac{\sigma_s}{4\pi}\phi_g + 3\sigma_{a,P}B_g - \frac{\sigma_s}{4\pi}\left(\nu\phi_\nu|_{\partial g}\right) - \left(\nu\sigma_a B_\nu|_{\partial g}\right)\right] \ ,\end{aligned} \tag{I.19}$$

for $g = 1, 2, \ldots, G$. Each equation of the RHD model (I.18) is an ordinary differential equation (ODE). Thus, this system can be reduced to simpler ODE expressions with boundary conditions and equations of state. The derivation of the reduced equations is outlined in the following chapter.

CHAPTER II

PROBLEM FORMULATION

Shock Problem Statement

Most of the assumptions made by Lowrie et. al are used in this work. We first assume a homogeneous medium. In order to close the system of equations, an equation of state (EOS) for the gas/medium is used. We assume a calorically perfect EOS given by the following relations:

$$P = \frac{\rho T}{\gamma} \ , \tag{II.1a}$$

$$e = \frac{T}{\gamma(\gamma - 1)} \ , \tag{II.1b}$$

where γ is the adiabatic index, the ratio of the specific heats of the material. It is also assumed to be constant and equal to 5/3. The ion and electron temperatures are also assumed to reach equilibrium instantaneously, which is equivalent to assuming that their temperatures are equivalent throughout the propagation of the shock. Heat conduction and viscous effects in the material have also been ignored. The multigroup approximation is applied to a constant opacity in order to investigate the structures of the group radiation temperatures. This model can certainly break down under conditions in which the aforementioned effects are no longer negligible. We assume a reference frame in which the shock speed is zero and the flow propagates in the +x direction. Quantities with a subscript-0 are in the pre-shock state which is attained as $x \to -\infty$. Far away from the shock, the flow is assumed to be in radiative equilibrium in which ($E_r = T^4$). The problem statement is summarized as

- Given: the constants γ, $\mathcal{M}_0$, $\mathbb{P}$, and the frequency-independent opacities σ_a and σ_t .
- Calculate:
  - The material properties $P(x)$, $\rho(x)$, $u(x)$, $T(x)$, and $\mathcal{M}(x)$.

– The radiation variables $I(\mu_m, x)$, $E_r(x)$, $F_r(x)$, $P_r(x)$, and $f(x)$ and their respective group quantities.

We now derive the reduced ODEs for the solution procedure in the same manner as was done by Ferguson [2]. Using the EOS, (II.1), the RHD equations can be re-expressed as

$$\partial_x(\rho u) = 0 \ , \tag{II.2a}$$

$$\partial_x \left(\rho u^2 + \frac{\rho T}{\gamma} + \mathbb{P} P_r \right) = 0 \ , \tag{II.2b}$$

$$\partial_x \left[u \left(\frac{1}{2}\rho u^2 + \frac{\rho T}{\gamma - 1} \right) + \mathbb{P}\mathbb{C} F_r \right] = 0 \ , \tag{II.2c}$$

$$\frac{\rho u}{\gamma(\gamma-1)\partial_x T} + \frac{\rho T}{\gamma}\partial_x u = -\mathbb{P}\mathbb{C}[\sigma_a(T^4 - E_r) + 2\sigma_a\beta(F_r - E_r - P_r)] \ . \tag{II.2d}$$

The steady-state multigroup S_n radiation transport equation is given by

$$\begin{aligned} \mu_m \partial_x I_{g,m} = \frac{\sigma_s}{4\pi}\phi_g + \sigma_{a,P} B_g - \sigma_{t,P} I_{g,m} - 2\frac{\sigma_s}{4\pi}\beta F_g + \frac{\sigma_s}{4\pi}\beta \left(\nu F_\nu|_{\partial g}\right) \\ +\mu_m\beta \left[\sigma_{t,P} I_{g,m} + I_{g,m}(\nu\partial_\nu\sigma_t)_{g,P} + 3\frac{\sigma_s}{4\pi}\phi_g + 3\sigma_{a,P}B_g - \frac{\sigma_s}{4\pi}\left(\nu\phi_\nu|_{\partial g}\right) - \left(\nu\sigma_a B_\nu|_{\partial g}\right) \right] \ , \\ m = 1, \ldots, N \ , \ g = 1, \ldots, G \ , \end{aligned} \tag{II.3}$$

which is the the multigroup radiation transport equation (I.19) discretized into N directions.

Derivation of the ODEs for the RHD Solve

Integrate (II.2a) to obtain

$$\rho u = u_0 \equiv \mathcal{M}_0 \tag{II.4}$$

where $\mathcal{M}_0$ is the initial shock Mach number. This velocity can thus be expressed in terms of the density as $u = \frac{\mathcal{M}_0}{\rho}$, which reduces the number of unknown variables to three in the rest of the RHD equations, which can thus be re-expressed as

$$\partial_x \left(\frac{\mathcal{M}_0^2}{\rho} + \frac{\rho T}{\gamma} + \mathbb{P} f E_r \right) = 0 \ , \tag{II.5a}$$

$$\partial_x \left(\mathcal{M}_0 \left[\frac{T}{\gamma(\gamma-1)} + \frac{1}{2}\frac{\mathcal{M}_0^2}{\rho^2} + \frac{T}{\gamma} + \mathbb{P}\left(\frac{\frac{\sigma_a}{\sigma_t}(fE_r + T^4) + \frac{\sigma_s}{\sigma_t}(1+f)E_r}{\rho} \right) \right] \right)$$
$$= \mathbb{P}\partial_x \left(\frac{\mathbb{C}^2}{\sigma_t} \partial_x (fE_r) \right) \ , \quad \text{(II.5b)}$$

$$\frac{\mathcal{M}_0}{\gamma(\gamma-1)}\partial_x T - \frac{\mathcal{M}_0 T}{\gamma\rho}\partial_x \rho = \mathbb{P}\sigma_a(E_r - T^4) \ . \quad \text{(II.5c)}$$

Integrate (II.5b), the conservation of energy equation, to obtain

$$\begin{aligned} \partial_x(fE_r) = & \frac{\sigma_t \mathcal{M}_0}{\mathbb{P}\mathbb{C}^2} \left[\frac{T-1}{\gamma-1} + \frac{\mathcal{M}_0^2}{2\rho^2}(1-\rho^2) \right. \\ & \left. + \mathbb{P}\left(\frac{\frac{\sigma_a}{\sigma_t}(fE_r + T^4) + \frac{\sigma_s}{\sigma_t}(1+f)E_r}{\rho} - \frac{4}{3} \right) \right] \ . \end{aligned} \quad \text{(II.6)}$$

The conservation of momentum equation, (II.5a), can be rewritten as

$$\left(\frac{T}{\gamma} - \frac{\mathcal{M}_0^2}{\rho^2} \right) \partial_x \rho + \frac{\rho}{\gamma}\partial_x T + \mathbb{P}\partial_x(fE_r) = 0 \ , \quad \text{(II.7)}$$

which can be used to solve for the spatial derivative of density

$$\partial_x \rho = \rho^2 \frac{\rho \partial_x T + \gamma \mathbb{P}\partial_x(fE_r)}{\gamma \mathcal{M}_0^2 - \rho^2 T} \ . \quad \text{(II.8)}$$

The material internal energy equation, (II.5c), can be re-expressed to solve for the spatial derivative of the material temperature

$$\partial_x T = \frac{\mathbb{P}(\gamma-1)}{\mathcal{M}_0 \rho(\mathcal{M}^2-1)} (\mathcal{M}_0 \partial_x(fE_r) + (\gamma\mathcal{M}^2 - 1)\rho\sigma_a(E_r - T^4)) \ . \quad \text{(II.9)}$$

The spatial derivative of density can now be rewritten in a more physically appealing form

$$\partial_x \rho = \frac{\mathbb{P}}{T\mathcal{M}_0(\mathcal{M}^2-1)[\mathcal{M}_0\partial_x(fE_r) + \rho\sigma_a(E_r - T^4)]} \ , \quad \text{(II.10)}$$

such that this form is aware of the shock location. Using the EOS (II.1), the local Mach number can be expressed as

$$\mathcal{M} = \frac{v}{\sqrt{T}} = \frac{\mathcal{M}_0}{\rho\sqrt{T}} \ . \tag{II.11}$$

The Mach number can now be treated as the independent variable by using (II.11)

$$\frac{dx}{d\mathcal{M}} = \frac{-2\rho T}{\mathcal{M}(2T\partial_x\rho + \rho\partial_x T)} \ , \tag{II.12}$$

which can be rewritten as

$$\begin{aligned} \frac{dx}{d\mathcal{M}} &= \frac{-2\rho T(\gamma\mathcal{M}^2 - 1)}{M(2\gamma\mathbb{P}\partial_x(fE_r) + (\gamma\mathcal{M}^2 + 1)\rho\partial_x T)} \\ &= \frac{-2\rho T\mathcal{M}_0(\mathcal{M}^2 - 1)}{\mathcal{M}\mathbb{P}(\gamma + 1)[\mathcal{M}_0\partial_x(fE_r) + (\frac{\gamma-1}{\gamma+1})(\gamma\mathcal{M}^2 + 1)\rho\sigma_a(E_r - T^4)]} \ . \end{aligned} \tag{II.13}$$

Equations (II.6) and (II.13) will be used for the solution procedure.

CHAPTER III

SOLUTION PROCEDURE

The procedure to obtain the solutions to the radiative shock problem is similar to what was implemented by Ferguson [2], with the main difference being the addition of the multigroup solve. The procedure is outlined as follows:

The First RHD Solve

1. Given the initial state, numerically determine the final state using the Rankine-Hugoniot jump conditions.
2. Initialize the ODE integration away from equilbrium and linearize away from the end-states.
3. Integrate the reduced ODEs through the precursor and relaxation regions away from $(T, P, \mathcal{M}, \dots)_\epsilon$ towards $\mathcal{M} = 1$.
4. Enforce continuity of the radiation flux (this is required because if the radiation flux is discontinuous, then the radiation energy is not conserved).

Transport Solve

1. Discretize the radiation variables I, E_r, F_r, and P_r into groups: I_g, E_g, F_g, and P_g
2. Initialize E_g and F_g according to their respective group Planck function, $E_g = \frac{B_g}{B} E_r$ and $F_g = \frac{B_g}{B} F_r$.
3. Solve the transport equation for all groups and for all angles, to determine $I_{g,m}$
4. Integrate $I_{g,m}$ along their direction cosines, μ_m.
5. Obtain the radiation variables E_r, F_r, and P_r from the radiation intensities $I_{g,m}$.

The Second RHD Solve

1. Set $P_\epsilon = P_{RT}(\mathcal{M}_\epsilon)$ using interpolation.

One iteration of this solution procedure is defined as going through the process as outlined above once. At the end of each iteration, L_2 and relative L_∞ errors for the radiation variables between the RHD and Transport solves are calculated. The L_2 and relative L_∞ errors are also computed for the VEF between each iteration. The solution procedure is terminated once the measured error no longer decreases after an iteration. It can also be terminated if the tolerance for the VEF has been satisfied. Once the solution has converged, then results for the material and radiation temperatures are analyzed.

CHAPTER IV

RESULTS

The equations (II.3), (II.6), and (II.13) were solved using Python. A benchmark test was used to determine if the multigroup code agreed with the results obtained from previous work by Lowrie and Edwards [3] and Ferguson [2]. We thus ran a shock problem using their assumptions which corresponds to grey non-equilibrium diffusion and grey-S_n transport. Our test problems thus takes the form of 1-group S_2 and S_n transport. This is because using one group in the multigroup approximation, is equivalent to a grey approximation and using S_2 transport is equivalent to the diffusion approximation. The results obtained using both of these methods are compared in Figure IV.1 for an initial Mach number of 1.2 ($\mathcal{M}_0 = 1.2$). The material temperature and radiation temperature obtained from grey non-equilbrium diffusion are denoted as T_{diff} and θ_{diff}, respectively. The material temperature and radiation temperature obtained from S_n transport are denoted as T, θ_{RH} and θ_{RT}.

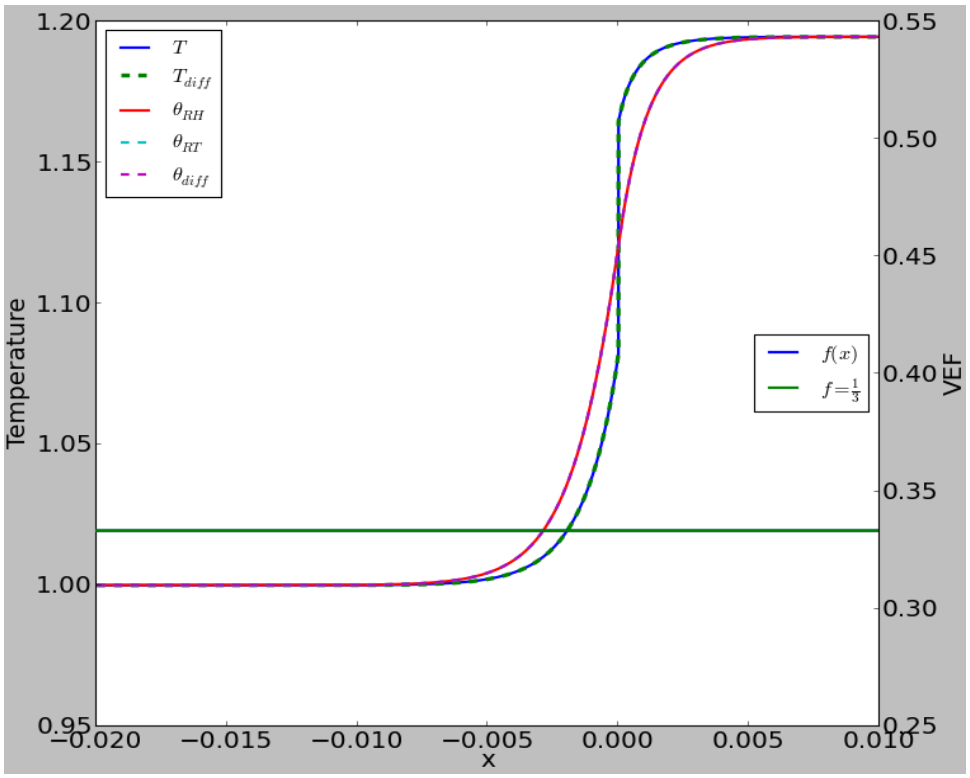

Fig. IV.1. Shock profile for the material and radiation temperatures for $\mathcal{M}_0 = 1.2$, S_2 (diffusion), and 1 group (grey). The VEF is overlayed and its values correspond to the right axis. The material and radiation temperatures obtained from grey non-equilibrium diffusion are plotted for comparison and the results are indistinguishable.

The shock interface is located at $x = 0$, and the equilibrium pre-shock temperature is achieved as $x \to -\infty$ and the equilibrium post-shock temperature is achieved as $x \to \infty$. The material and radiation temperatures are in equilibrium "far away" from the shock interface. The comparison shows that our solutions for 1-group S_2 transport are indistinguisable from those obtained by using grey non-equilibrium diffusion. The VEF is 1/3 over the shock domain, which indicates that the solution is in the diffusion regime. The same type of problem was run using 2 groups to ensure that the multigroup method would converge and produce the same solution. See Figure IV.2

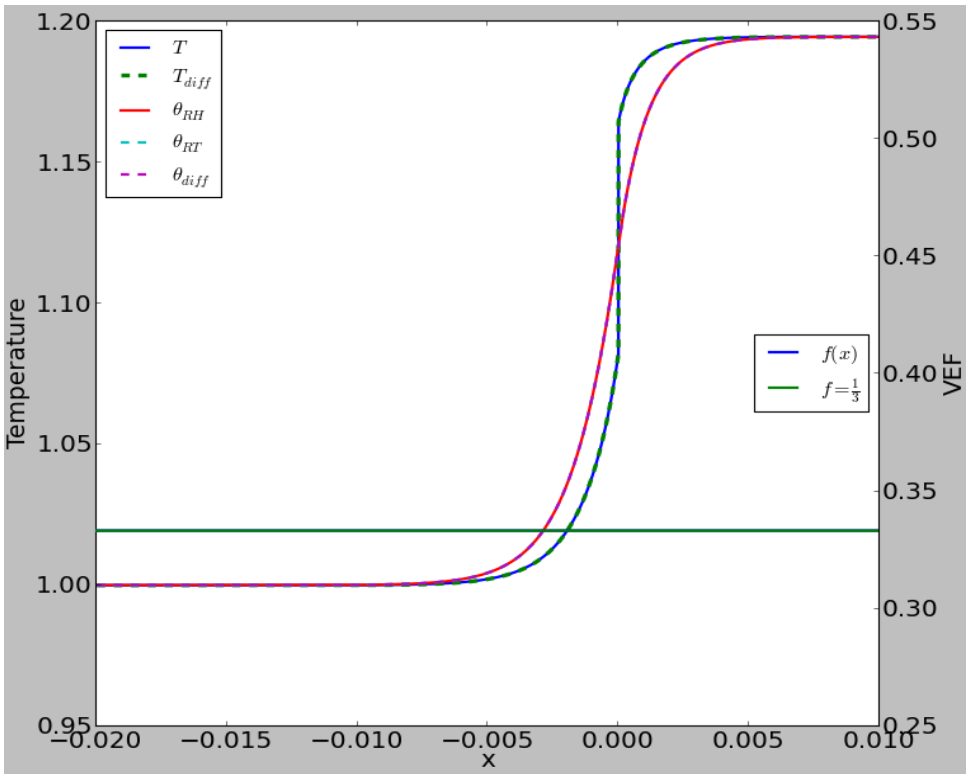

Fig. IV.2. Shock profile for the material and radiation temperatures for S_2 (diffusion), 2 groups, and $\mathcal{M}_0 = 1.2$.

The results shown in Figure IV.2 exhibit the exact same profile as obtained in Figure IV.1, which confirms that the multigroup method is indeed consistent. Temperature profiles for higher Mach numbers, a higher number of groups, and higher orders of S_n are now presented. The shock profile for a constant opacity using S_4, 5 groups, and $\mathcal{M}_0 = 2.0$ is given in Figure IV.3.

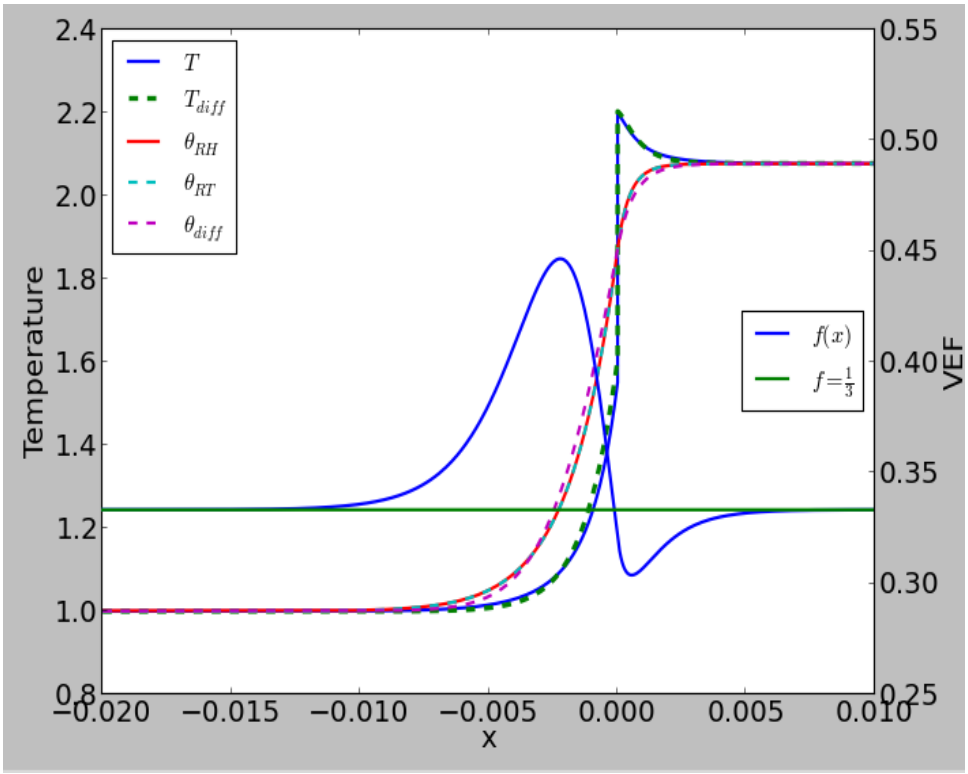

Fig. IV.3. Material and radiation temperature shock profiles for S_4, 5 groups, and $\mathcal{M}_0 = 2.0$.

The VEF is shown to be $> 1/3$ in the precursor region and is shown to be $< 1/3$ in the cooling layer, which is expected.

We begin our investigation of the structure of the group radiation temperatures by first looking at the Planck function, which dictates which groups contribute most to the total radiation temperature.

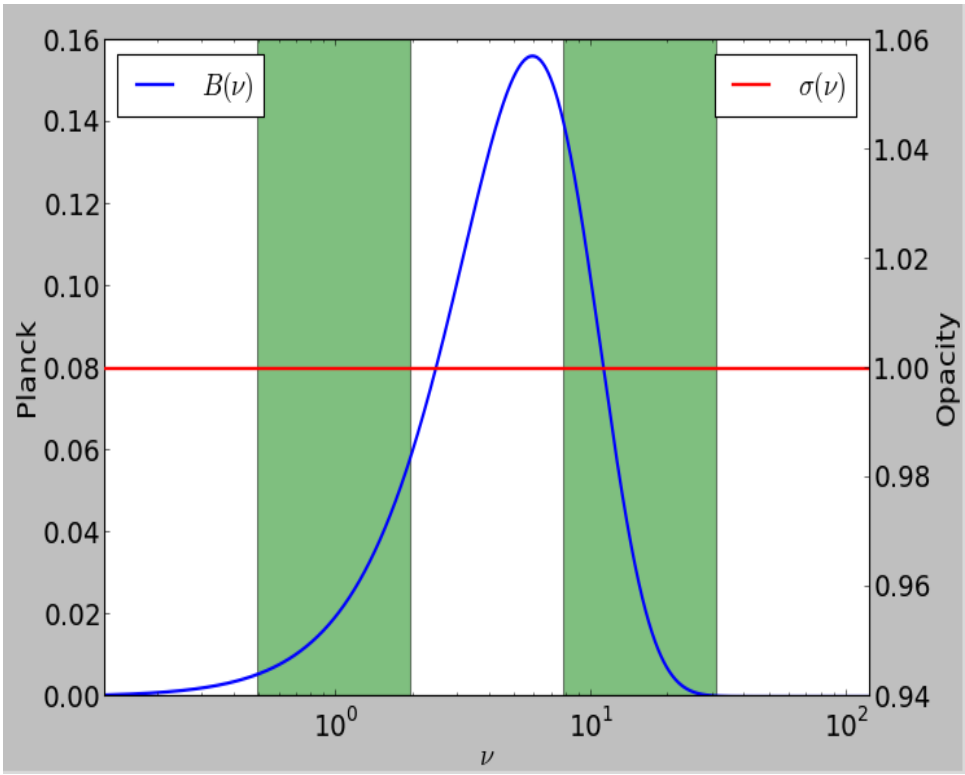

Fig. IV.4. Nondimensionalized Planck function overlayed with an opacity with a constant dependence on frequency. The frequency spectrum is discretized into 5 groups, which are indicated by the alternating white and green bars. The group endpoints are located at the interface between the white and green bars.

In Figure IV.4, the Planck function is shown to be dominant in groups 3 and 4, while the groups ends, 1 and 5, have little to no contribution. Since we implement a frequency-independent opacity, the Planck group structure is preserved. If the opacity is frequency-dependent, then groups where the opacity is relatively large may start to have a significant contribution to radiation emission, which will affect the structure of the group radiation temperatures. Multigroup is now applied for a constant opacity profile in order to determine what groups dominate the radiation temperature, θ_{RT}. The frequency domain was discretized into 5 groups and the radiation temperature for each group (θ_{RT_g}) is plotted in Figure IV.5.

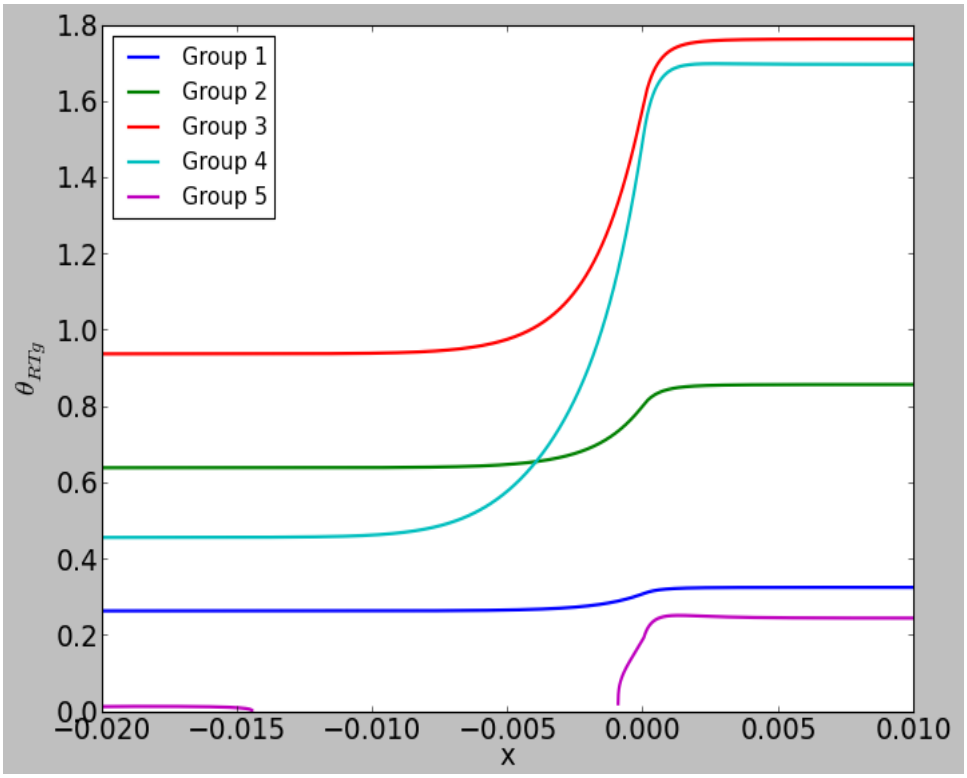

Fig. IV.5. Nondimensionalized group radiation temperatures for S_4, 5 groups, and $\mathcal{M}_0 = 2$.

For the group radiation temperatures, we see that groups 3 and 4 are dominant, followed by groups 2, 1, and 5, respectively. This agrees with the group structure of the Planck function in Figure IV.4. We now investigate the group radiation temperature structures for shock profiles that exhibit anti-diffusive-like behavior. Shocks for $\mathcal{M}_0 = 3$ are known to exhibit anti-diffusive-like behavior when using transport to describe the radiation field, which was shown by Ferguson [2]. See Figure IV.6.

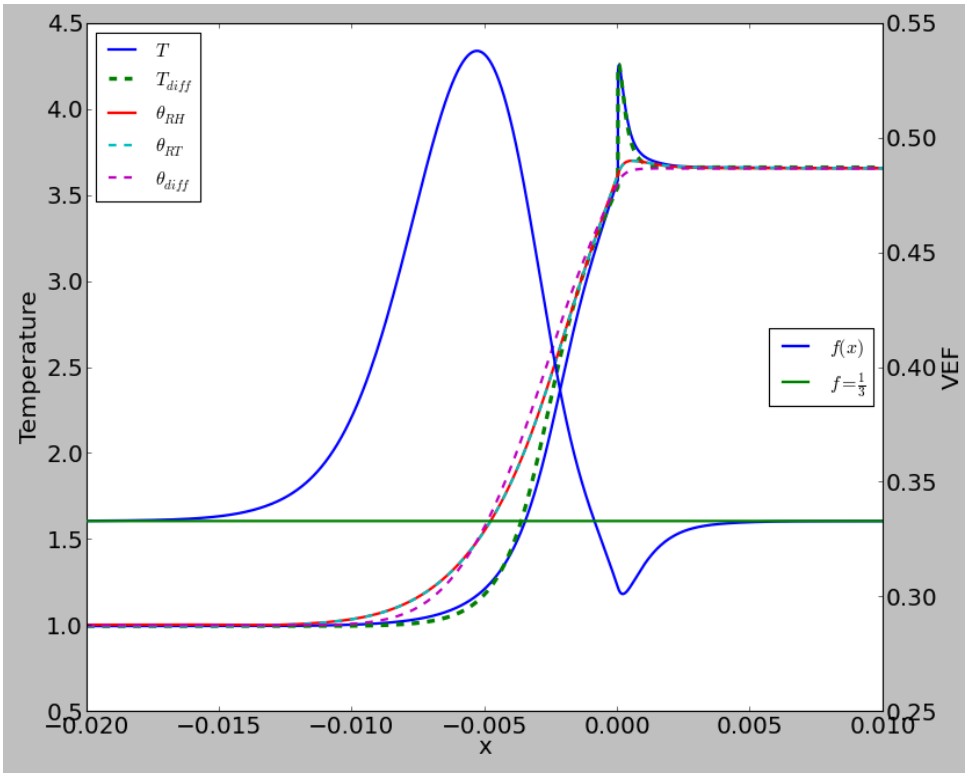

Fig. IV.6. Material and radiation temperature profiles for S_4, 5 groups, and $\mathcal{M}_0 = 3$.

This is represented by the small peak, where as in the diffusion case represented by the purple-dashed line, the radiation temperature monotonically increases over the shock domain. The VEF again shows where the precursor region and cooling layer are located. We now investigate the group structure of the radiation temperature and show that anti-diffusive-like behavior can occur for the frequency-dependent nonequilibrium diffusion model. The frequency domain is now discretized into 10 groups as shown in Figure IV.7.

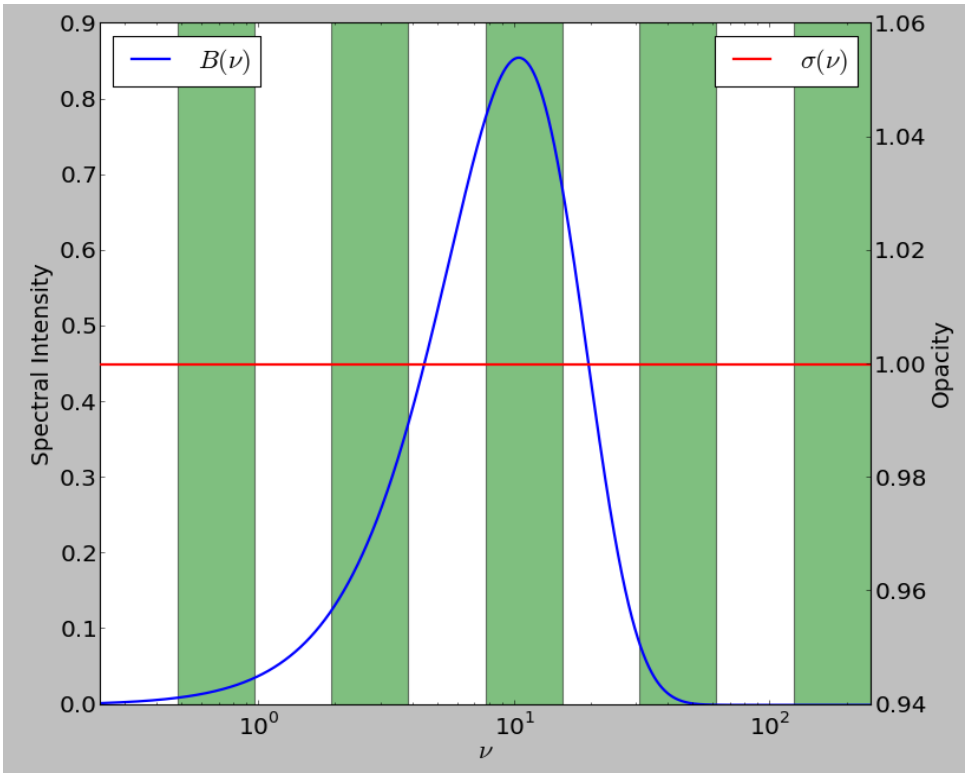

Fig. IV.7. Nondimensionalized Planck function overlayed with constant opacity profile for S4, 10 groups, and $\mathcal{M}_0 = 3$.

Groups 5, 6, and 7 are shown to dominate the other groups. The group radiation temperatures are plotted in Figure IV.8 and we see that groups 5, 6, and 7 indeed dominate all of the other groups.

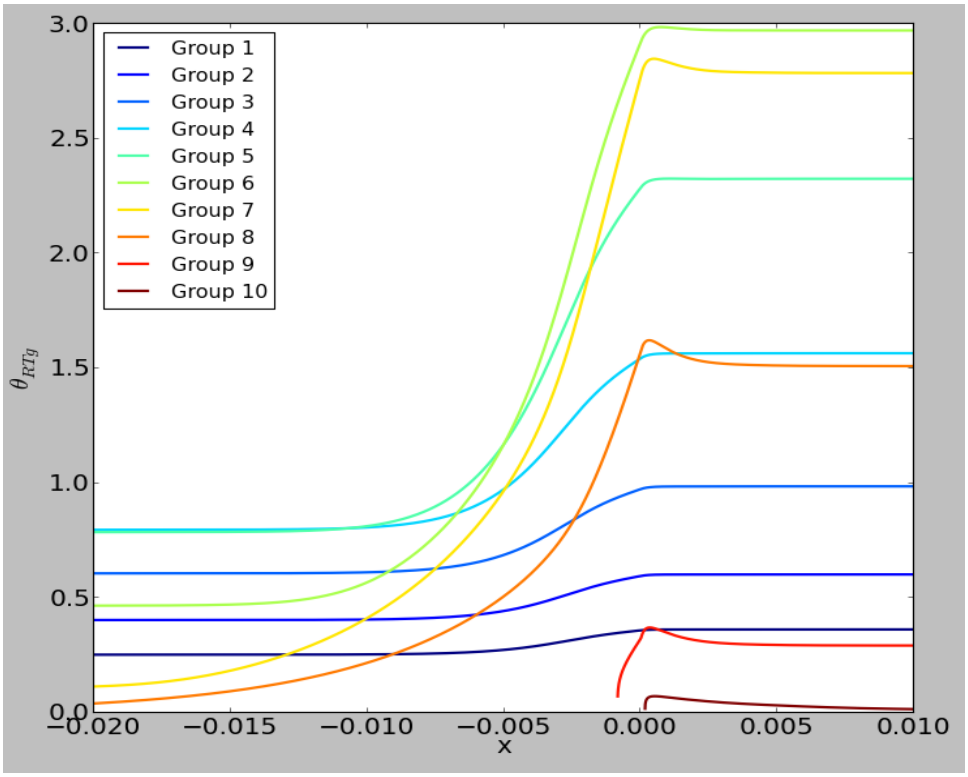

Fig. IV.8. Group radiation temperature profiles for S_4, 10 groups, and $\mathcal{M}_0 = 3$.

More importantly, we note that the lower groups do not exhibit anti-diffusive-like behavior, while the higher groups do. We note a peak in group 6 in the cooling layer, and this feature starts to become more apparent for higher groups. We now consider the 20-group case for higher resolution of the frequency spectrum.

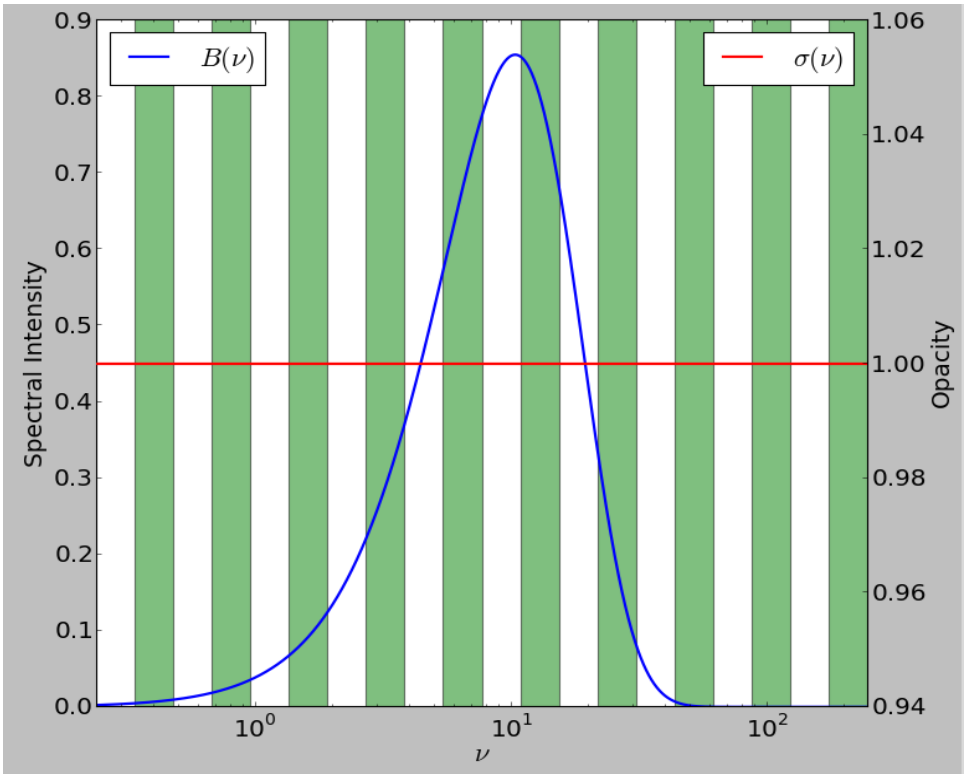

Fig. IV.9. Nondimensionalized Planck function overlayed with constant opacity profile for S4, 20 groups, and $\mathcal{M}_0 = 3$.

The Planck function is discretized over the 20 groups in Figure IV.9 and again indicates which groups are expected to dominate the radiation temperature, which is presented in Figure IV.10.

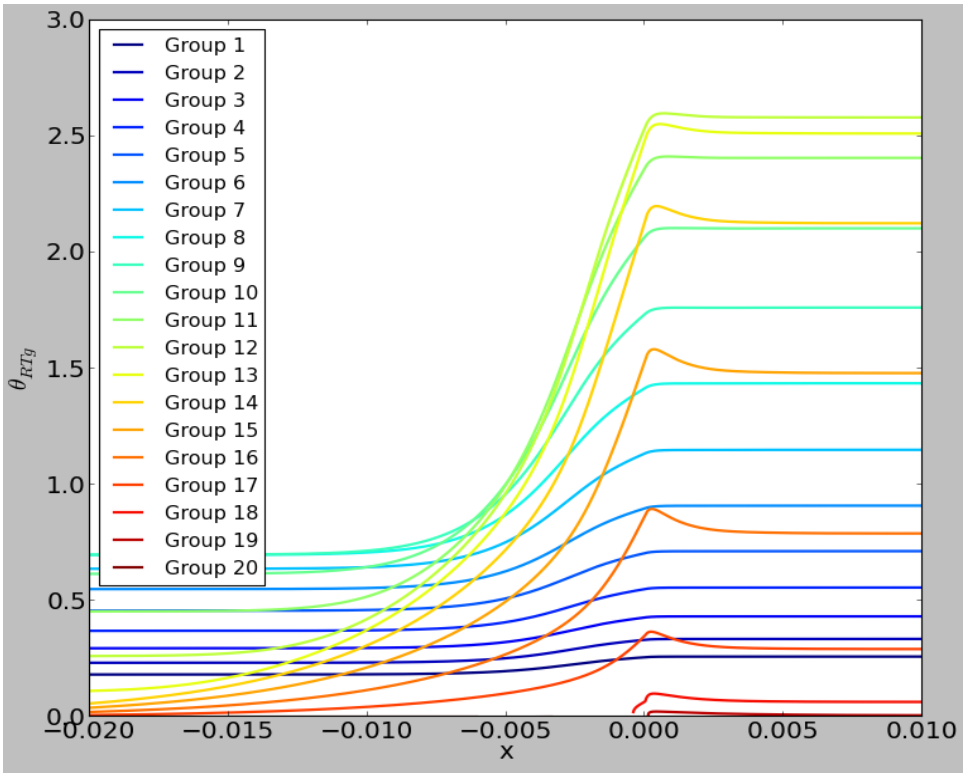

Fig. IV.10. Group radiation temperature profiles for S_4, 20 groups, and $\mathcal{M}_0 = 3$.

When 20 groups are used, the same trend is achieved. The lower groups increase monotonically, while for groups 11 and higher, the group radiation temperatures exhibit anti-diffusive-like behavior.

We now implement S_2, which is equivalent to diffusion. This, in effect, removes the angular dependence of the radiation field. The group radiation temperatures are plotted for 20 groups in Figure IV.11.

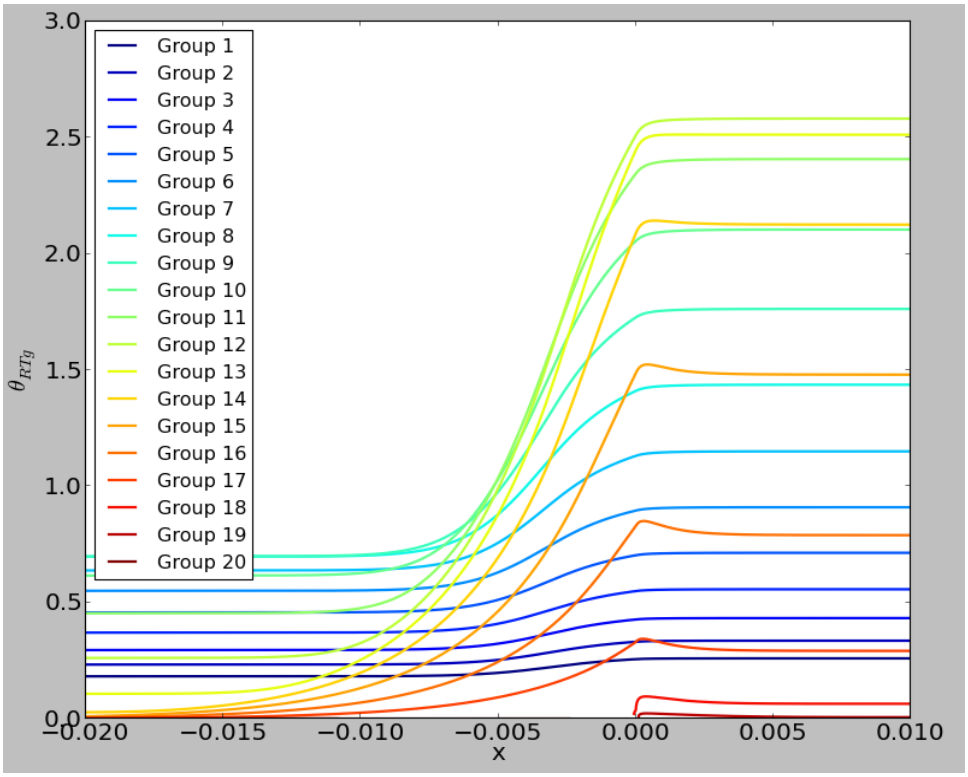

Fig. IV.11. Group radiation temperature profiles for S_2, 20 groups, and $\mathcal{M}_0 = 3$.

Anti-diffusive-like behavior begins to become apparent for group 14 when using S_2 (diffusion), as opposed to group 13 for $_4$. The peaks are not as sharp as those for S_4, but they are indeed significant for explaining the underlying physics. This implies that anti-diffusive-like behavior may occur for frequency dependence and not just angular dependence, as previously thought.

CHAPTER V

CONCLUSIONS

We obtained semi-analytic solutions to radiative shock waves using a multigroup S_n transport model and a constant opacity. Our multigroup solutions agree with previous grey solutions by Lowrie and Edwards [3] and Ferguson [2]. We have shown that when the radiation temperature is discretized into frequency groups, higher groups may exhibit anti-diffusive-like behavior. This was shown for runs using S_n transport and diffusion. The results we have obtained imply that the frequency dependence of the Planck function plays a role in anti-diffusive-like behavior in radiative shock waves and not just the angular dependence of the radiation field.

Future Work

Further investigation of these results and implications will be the focus of future work. Frequency-dependent analytic opacities will then be implemented in our multigroup S_n transport model in order to determine what effect they have on radiative shock structures.

REFERENCES

[1] R. Paul Drake. *High-Energy-Density Physics*. Springer-Verlag, New York, 2006.

[2] Jim M. Ferguson. *Asymptotic Accuracy of the Equilibrium Diffusion Approximation and Semi-Analytic Solutions of Radiating Shocks*. PhD thesis, Texas A&M University, 2014.

[3] R. B. Lowrie and J. D. Edwards. Radiative shock solutions with grey nonequilibrium diffusion. *Shock Waves*, 18:129–143, 2008.

[4] R. B. Lowrie and R. M. Rauenzahn. Radiative shock solutions in the equilibrium diffusion limit. *Shock Waves*, 16:445–453, 2007.

[5] Ryan G. McClarren and R. Paul Drake. Anti-diffusive radiation flow in the cooling layer of a radiating shock. *Journal of Quantitative Spectroscopy & Radiative Transfer*, 111, 2010.

[6] D. Mihalas and B.W. Mihalas. *Foundations of Radiation Hydrodynamics*. Oxford University Press, New York, 1984.

[7] Annamaneni Peraiah. *An Introduction to Radiative Transfer: Methods and Applications in Astrophysics*. Cambridge University Press, Cambridge, United Kingdom, 2004.

[8] N. Vaytet et al. The influence of frequency-dependent radiative transfer on the structures of radiative shocks. *Journal of Quantitative Spectroscopy & Radiative Transfer*, 125, 2013.

[9] R. B. Williams. *Adaptive Multigroup Radiation Diffusion*. PhD thesis, Massachusetts Institute of Technology, 2005.